e-ISSN: 2550-164X

Available online at
https://jmeche.uitm.edu.my/

Journal of Mechanical Engineering 23(3) 2026, 70 – 93.

Journal of Mechanical Engineering

Enhancing the Thermal Performance of an Evacuated Tube Solar Collector using CuO Nanofluids

Kashif Waseem[1*], Ahmed N. Oumer[1], Rehan Ahmed[1]

[1]*School of Engineering and Physical Sciences, Heriot Watt University Dubai, Dubai, UAE*

ARTICLE INFO

Article history:
Received 2 December 2025
Revised 3 May 2026
Accepted 26 May 2026
Published 15 September 2026

Keywords:
ETSC
Thermal performance
Nanofluids
CFD
Parametric optimization

DOI:
10.24191/jmeche.v23i3.9739

ABSTRACT

With the growing adoption of Evacuated Tube Solar Collectors (ETSCs), enhancing their thermal performance remains a critical challenge. Nanofluids have shown strong potential to enhance heat transfer, yet the optimal nanoparticle input parameters for maximizing collector efficiency remain poorly understood. This study investigates the use of CuO/50:50 ethylene glycol–water (EG–water) nanofluids to improve heat transfer and thermal efficiency in ETSCs through a novel and comprehensive experimental, computational and parametric optimization approach. Baseline experiments with 50:50 EG–water provide validation for a Computational Fluid Dynamics (CFD) model, which is then simulated with CuO nanofluids to investigate how variations in Reynolds number, nanoparticle volume concentration and irradiance affect ETSC thermal performance. The results demonstrate that a 5% CuO nanoparticle volume concentration enhances the Nusselt number by 34% and improves collector thermal efficiency by 13.5%, albeit with a 21% increase in skin friction coefficient. The optimal operating conditions occur at Re = 850, ϕ = 5%, I = 1000 W/m^2 and T_I = 268 K, yielding a high Nusselt number of 62.6 and a low skin friction coefficient of 0.0359. These findings demonstrate the strong potential of employing CuO nanofluids in ETSCs to enhance their thermal performance.

Nomenclature

A_{col}	Absorber Area (m^2)	T_1	Fluid Inlet Temperature (℃)
c	Specific Heat ($J\ kg^{-1}$)	T_2	Fluid Outlet Temperature (℃)
g_y	Gravity in the y-Direction (ms^{-2})	T_m	Mean Fluid Temperature (℃)
I	Irradiance (Wm^{-2})	T_{amb}	Ambient Temperature (℃)
k	Thermal Conductivity ($Wm^{-1}K^{-1}$)	u_x	Velocity in the x-Direction (ms^{-1})
$\dot{V}$	Volumetric Flow Rate (m^3s^{-1})	u_y	Velocity in the y-Direction (ms^{-1})
P	Pressure (Pa)	u_z	Velocity in the z-Direction (ms^{-1})
$\dot{Q}_{in}$	Heat Input (W)		
$\dot{Q}_u$	Useful Heat (W)		

[1*] Corresponding author. *E-mail address*: kw2036@hw.ac.uk
https://doi.org/10.24191/jmeche.v23i3.9739

©Kashif Waseem et al., 2026

Introduction

The growing concerns over energy sustainability and environmental impact have accelerated the global adoption of renewable energy technologies worldwide, with recent decades showing a clear rise in renewable energy consumption (Raimi et al., 2023; Solangi et al., 2011). Among these technologies, solar energy stands out as a clean, abundant, and reliable energy source, with solar collectors playing a central role in converting solar radiation into usable thermal energy (Aggarwal et al., 2023; Kannan & Vakeesan, 2016). Among solar collectors, Evacuated Tube Solar Collectors (ETSCs) are widely regarded as having the best thermal performance due to their superior thermal efficiency and reduced heat losses (Ayompe & Duffy, 2013; Mangal et al., 2010; Zubriski & Dick, 2012). Despite these advantages, their performance remains constrained by the thermal properties of conventional heat transfer fluids, such as water and oil-based fluids, which possess relatively low thermal conductivity (Cheng et al., 2013; Nie et al., 2020). This limitation restricts the collector's ability to achieve optimal thermal efficiency (Kalogirou, 2004; Morrison et al., 2004). Advancements in nanotechnology have introduced nanofluids as potential solutions to enhance the heat transfer characteristics of the collector working fluid due to their superior thermal conductivity (Olfian et al., 2020). A review of the simulation studies investigating the use of nanofluids in ETSCs revealed that there are three main factors affecting the thermal performance of the collector: nanoparticle volume concentration, nanoparticle type and mass flow rate. Table 1 summarizes 12 simulation studies that vary these parameters to evaluate their effects on collector efficiency and overall heat transfer enhancement.

Table 1. Summary review of simulation studies investigating nanofluids in ETSCs

Author & Year	Nanofluid	Mass Flow Rate	Volume Concentration	Finding
(Kim et al., 2016)	MWCNT, Al_2O_3, CuO, TiO_2, SiO_2	0.001 kg/s to 0.01 kg/s	1% to 3% 0.1% to 0.2% (MWCNT)	Thermal efficiency enhancement in order of greatest to least: MWCNT, CuO, Al_2O_3, TiO_2, SiO_2
(Yan et al., 2017)	SiO_2	-	1%, 3%, 5%	Highest thermal conductivity increase of the working fluid was 45%.
(Sadeghi et al., 2019)	Cu2O	-	0.04% and 0.08%	Maximum efficiency of the collector was 78% at 0.08 vol% compared to 74% without nanofluid.
(Kaya & Arslan, 2019)	Ag, ZnO and MgO	0.001 kg/s and 0.003 kg/s	1% to 4%	Maximum collector efficiency was 68.6% for 4 vol% of Ag/water, which is 26.7% higher than without nanofluids.
(Mercan & Yurddaş, 2019)	CuO and Al_2O_3	0.025 kg/s to 0.075 kg/s	1%, 3%, 5%	Greatest heat transfer enhancement was 6.8% for CuO/water at 5 vol%.
(Yurddaş, 2020)	MWCNT, Cu, TiO_2, and SiO_2	0.05 kg/s	0.5% to 5%	Highest increase in heat transfer was 14.1% for Cu/water at 5 vol%.
(Peng et al., 2020)	Al_2O_3, CuO, TiO_2	0.005 kg/s	0.1% to 4%	CuO/water has the highest thermal efficiency increase compared to water of 13.8%.
(Hasan et al., 2022)	SiO_2	-	1% to 4%	Maximum enhancement of the average Nusselt number was 42% at 4 vol% and $Re = 30000$ compared to without nanofluids.
(Tabarhoseini & Sheikholeslami, 2022)	MWCNT and Cu	-	1%, 3%, 5%	Thermal efficiency of the collector was enhanced by 2% and 2.73% by the Cu and MWCNT particles respectively at 5 vol%.

https://doi.org/10.24191/jmeche.v23i3.9739

©Kashif Waseem et al., 2026

(López-Núñez et al., 2022)	TiO_2	0.02475 kg/s to 0.1188 kg/s	0.5%	Highest collector efficiency (90%) achieved at 0.1188 kg/s using TiO_2 /water - compared to 86% without nanofluids.
(López-Núñez et al., 2024)	TiO_2 and SiO_2	0.04818 kg/s to 0.1188 kg/s	0.5%	Highest thermal efficiency of the collector was 86% using TiO_2 /water at 0.1188 kg/s compared to 80% without nanofluids.
(Aytaç et al., 2024)	Quartz /water	0.008 kg/s to 0.050 kg/s	2%	At mass flow rate of 0.05 kg/s the greatest thermal efficiency of 75.63% was recorded compared to using water (58.55%).

Yan et al. (2017) designed and simulated an ETSC using water/SiO_2 nanofluids for volume concentrations of 1%, 3% and 5% to determine the heat transfer improvement. Their results showed that the highest thermal conductivity increase was 45% at 5 vol%. Sadeghi et al. (2019) numerically investigated how nanoparticle volume concentration affects the performance of an ETSC equipped with a parabolic reflector, employing Cu_2O/DW nanofluids. They reported a maximum collector efficiency of 78% at 0.08 vol%, compared to 74% for pure water. Hasan et al. (2022) examined the influence of nanoparticle volume concentration and particle diameter on the Nusselt number and skin friction factor using water/SiO_2 nanofluids. They found that higher concentrations and smaller nanoparticle diameters significantly increased heat transfer, with a maximum average Nusselt number enhancement of 42% at 4 vol% and Re = 30,000. Tabarhoseini & Sheikholeslami (2022) scrutinized the effect of water-based MWCNT and Cu nanoparticles on the efficiency of the collector at different volume concentrations. They determined that the thermal efficiency of the collector was enhanced by 2% and 2.73% by the Cu and MWCNT particles respectively at 5 vol%. Taken together, these four studies demonstrate that increasing nanoparticle volume concentration consistently improves ETSC thermal performance. Most studies limited the concentration to 5% due to stability concerns, establishing this as a practical upper threshold for nanofluid applications.

Kaya & Arslan (2019) designed and simulated an ETSC using Ag, ZnO, and MgO nanofluids with ethylene-glycol/water as the base fluid. They reported the highest efficiency of 68.6% using 4 vol% Ag nanofluids, corresponding to a 26.7% improvement over the base fluid. Yurddaş (2020) modelled ETSC performance using water-based MWCNT, Cu, TiO_2, and SiO_2 nanofluids at concentrations from 1%–5%. The study found that Cu nanofluids produced the highest heat transfer enhancement of 14.1% at 5 vol%. Peng et al. (2020) dedicated their research to studying the effects of water based Al_2O_3, CuO, TiO_2 nanofluids on the thermal performance of the collector. At 0.005 kg/s, CuO/water yielded the highest efficiency increase of 13.8%, outperforming TiO_2/water by 1.5% and Al_2O_3/water by 1.3%. Kim et al. (2016) numerically investigated hybrid MWCNT, Al_2O_3, CuO, TiO_2, SiO_2 nanofluids using a 20% PG-water base fluid. They found that the collector thermal efficiency increased in the following sequential order from greatest to least: MWCNT, CuO, Al_2O_3, TiO_2, SiO_2. The highest thermal collector efficiency increases of 10.5% was reported for 0.2 vol% MWCNT. Across these four studies, copper-based nanoparticles outperformed Al_2O_3, TiO_2 and SiO_2 at equivalent concentrations, indicating that they are the most effective at enhancing the thermal efficiency of the collector. However, more research is required to compare Copper nanoparticles with MWCNTs, which also demonstrated significant potential.

Mercan & Yurddaş (2019) examined the effects of CuO and Al_2O_3 nanofluids on ETSC heat transfer at various mass flow rates, identifying the optimal flow rate as 0.025 kg/s. Their maximum enhancement was 6.8% for 5 vol% CuO/water. López-Núñez et al. (2022) numerically analysed TiO_2/water nanofluids across a flow-rate range of 0.02475 to 0.1188 kg/s. They achieved a maximum collector efficiency of 90% using TiO_2/water at 0.1188 kg/s, compared to 86% for water. In a follow-up study (López-Núñez et al., 2024), they compared SiO_2 and TiO_2 nanofluids under similar conditions and again observed superior performance using TiO_2/water, reaching a collector thermal efficiency of 86% at 0.1188 kg/s versus 80%

https://doi.org/10.24191/jmeche.v23i3.9739

©Kashif Waseem et al., 2026

for pure water. Aytaç et al. (2024) conducted numerical and experimental investigations using Quartz/water nanofluids to determine the effect of mass flow rate on ETSC thermal performance. They found that higher mass flow rates consistently increased collector thermal efficiency, with Quartz/water achieving an efficiency of 75.63% at 0.05 kg/s compared to 58.55% for water. Collectively, these four studies confirm that increasing mass flow rate enhances ETSC thermal efficiency due to improved convective heat transfer. This trend is consistent across nanofluids and pure water, establishing flow rate as a key operational parameter for performance optimisation.

The literature has shown that Al_2O_3 and CuO are the most used nanoparticles in ETSC simulation studies (Kim et al., 2016; Mercan & Yurddaş, 2019; Peng et al., 2020). Figs. 1 and 2 present the corresponding thermal efficiency enhancements at various volume concentrations across three representative studies. For both nanofluids, thermal efficiency increases linearly with concentration. Differences in collector geometry influenced performance as Peng et al. (2020) reported the largest efficiency gains, likely due to simulating a 94 mm diameter collector compared to the 37 mm configuration used by Mercan & Yurddas (2019). Across all studies, CuO demonstrated consistently higher efficiency enhancement than Al_2O_3. Peng et al. (2020) reported the highest improvements, with maximum thermal efficiency increases of 13.8% for CuO and 9.3% for Al_2O_3 under comparable conditions. These findings collectively indicate that CuO is not only one of the most widely used nanoparticles but also the most effective in improving ETSC thermal performance.

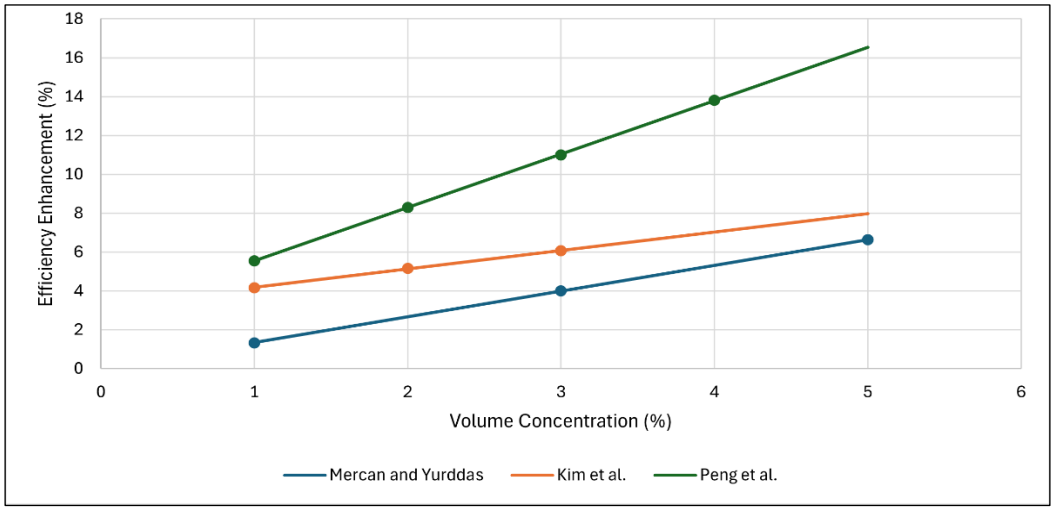


Fig. 1. Thermal efficiency enhancement of ETSC using CuO nanofluids at various volume concentrations reported by different authors.

https://doi.org/10.24191/jmeche.v23i3.9739

©Kashif Waseem et al., 2026

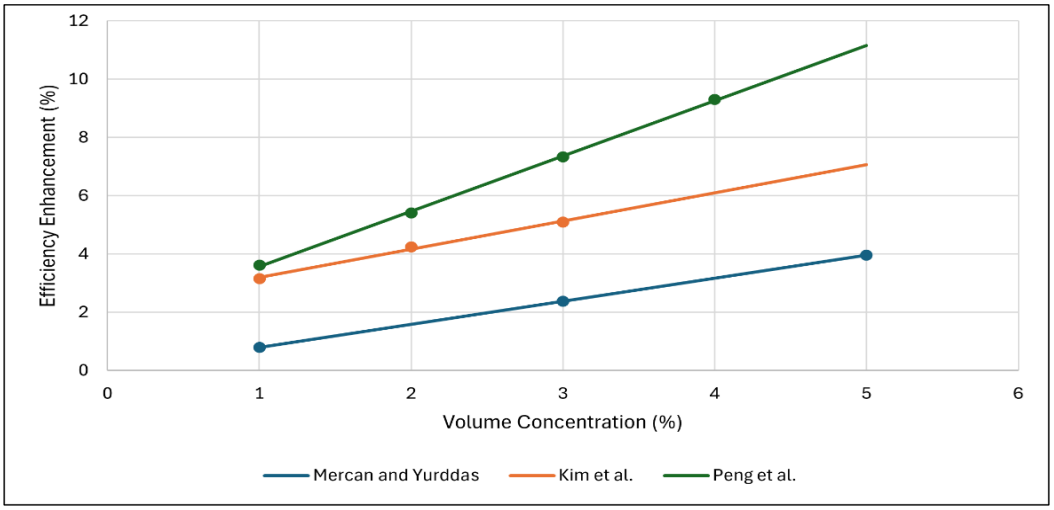


Fig. 2. Thermal efficiency enhancement of ETSC using Al_2O_3 nanofluids at various volume concentrations reported by different authors.

Current experimental studies on ETSCs lack detailed insight into key heat transfer mechanisms, such as nanoparticle conductivity and internal temperature distribution (Pawar & Sobhansarbandi, 2020). While computational studies have advanced the understanding of nanofluid behaviour, they largely focus on isolated parameter variations and lack a systematic, multi-variable optimization framework to identify optimal operating conditions (Aggarwal et al., 2023; Olfian et al., 2020). Moreover, the integration of parametric optimization techniques remains largely unexplored, representing a critical gap in the practical application of nanofluids in ETSCs (Jaiswal et al., 2023; Sood et al., 2026). To address these limitations, this study employs parametric optimization using Design of Experiments (DOE) to develop predictive second-order models and facilitate the optimization of multiple interacting parameters, including nanoparticle concentration and operating conditions. Unlike prior studies, this methodology allows for the identification of global optimal nanoparticle parameters rather than localized trends. Additionally, CFD is employed to analyze nanofluid thermal and flow behaviour in ETSCs, providing detailed insights such as temperature fields and flow patterns which are not easily attainable experimentally. In doing so, the study bridges the gap between theoretical developments in nanofluid technology and their practical application in enhancing the thermal performance of ETSCs.

The main objectives of this study are (1) To develop and experimentally validate a CFD model of the ETSC in ANSYS Fluent. (2) To investigate the thermal performance enhancement of the ETSC by simulating the CFD model with nanofluids by varying key parameters such as the Reynolds number, nanoparticle volume concentration and irradiance. (3) To optimize the model according to different operating parameters such as Reynolds number, nanoparticle volume concentration, irradiance and fluid inlet temperature.

Methodology

Experimental setup

The first objective of the study requires the collection of experimental data with the ETSC. The collector's performance was investigated at flow rates of 16 l/h, 28 l/h and 41.5 l/h and collector tilt angles

https://doi.org/10.24191/jmeche.v23i3.9739

©Kashif Waseem et al., 2026

of 30°, 40° and 50° across three different days during the summer between 10 am to 2 pm to ensure consistent solar irradiation. The copper heat pipes in the glass tubes absorb the incoming solar irradiation and transmit this energy to the working fluid (50:50 EG-Water) in the manifold pipe. The working fluid is then pumped to the heat exchanger where it heats water in the secondary circuit before returning to the collector.

Table 2 presents the ETSC's specifications, while Fig. 3 shows a schematic of its components. As depicted, TS4 and TS1 are the measured inlet and outlet fluid temperatures respectively, and these values are displayed by the UVR67 controller. The controller also displays the volumetric flow rate (RS5) and the illuminance (FS6). These parameters are then recorded by the data logger using Winsol software. The ambient temperature, T5, and the system pressure, P1, are recorded manually from their respective gauges as seen in Figs. 3 and 4.

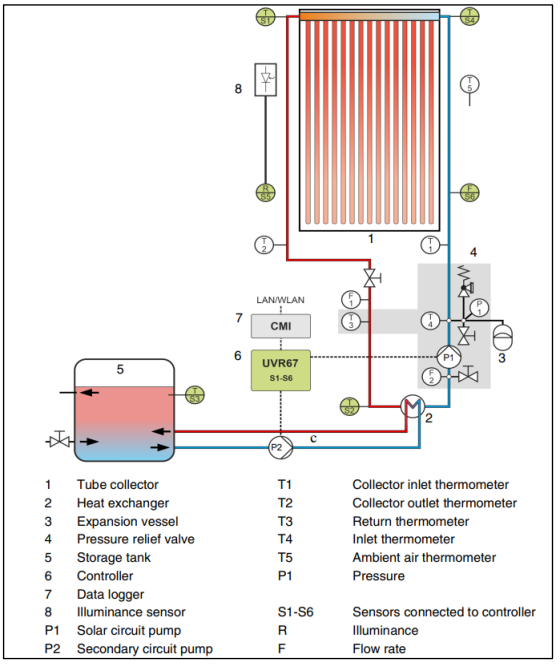


Fig. 3. Schematic of the investigated ETSC.

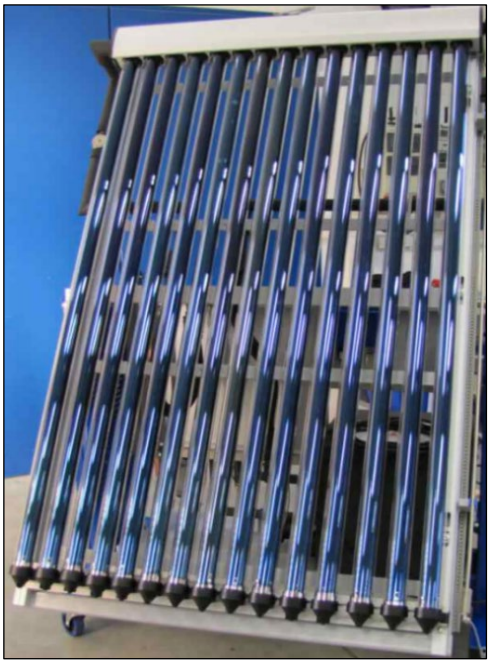


Fig. 4. Image of the ETSC analyzed in this study.

Table 2. Specification of the investigated ETSC

Manifold Pipe Length (mm)	1200
Manifold Pipe Outer Diameter (mm)	42
Manifold Pipe Inner Diameter (mm)	40
Manifold Pipe Material	Copper
Number of Heat Pipes	15
Heat Pipe Diameter (mm)	8
Heat Pipe Condenser Diameter (mm)	24

https://doi.org/10.24191/jmeche.v23i3.9739

©Kashif Waseem et al., 2026

Simulation setup

Mathematical formulae and assumptions

The second objective of the study involves the investigation of the thermal performance of the ETSC using CuO nanofluids through CFD analysis and is conducted under specific assumptions to simplify the simulation procedure. Heat transfer between the ethanol within the evacuated tubes and the working fluid in the manifold pipe is modelled with heat losses, consistent with the experimental setup. These losses are incorporated through an appropriate heat loss factor within the governing energy equations in both the experimental analysis and CFD model.

For nanofluid modelling, a single-phase approach is employed, assuming homogeneous dispersion of CuO nanoparticles within the base fluid. This approach has been widely reported to yield accurate computational results, particularly at low nanoparticle volume concentrations (Mercan & Yurddaş, 2019; Peng et al., 2020). This assumption is justified by the negligible effects of slip velocity and particle migration effects under such conditions. The effective thermophysical properties of the nanofluid are calculated using established correlations, which have been extensively validated and are commonly applied in CFD-based nanofluid studies (Brinkman, 1952; Khanafer et al., 2003; Maxwell, 1873). Furthermore, the thermophysical properties of the working fluid are assumed to be constant over the investigated temperature range, which is relatively narrow. This assumption is consistent with prior studies and has been shown to provide reliable results (Aytaç et al., 2024; Sadeghi et al., 2019; Yurddaş, 2020). In addition, the Boussinesq approximation is employed, whereby density variations are considered only in the buoyancy term, while all other fluid properties remain constant.

The limitation of nanoparticle concentration to 5% has been justified based on previous studies in literature as higher concentrations may lead to stability issues such as agglomeration and sedimentation (Tabarhoseini & Sheikholeslami, 2022; Yan et al., 2017). The study solely examines the simulation procedure of using CuO nanofluids to enhance the thermal performance of the ETSC, excluding experimental setups using nanofluids. Furthermore, aspects related to simulation settings, such as residual behaviour, discretization techniques, and numerical stability, fall outside the scope of this study.

With these assumptions, the efficiency of the collector can be calculated by considering the power input to the collector and the useful power output. The rate of thermal energy transferred to the collector is:

$$\dot{Q}_{in} = IA_{Col} \tag{1}$$

The useful power output of the collector is:

$$\dot{Q}_u = \dot{V}\rho c_p(T_2 - T_1) \tag{2}$$

Thus, the efficiency of the collector is denoted as:

$$\eta = \frac{\dot{Q}_u}{\dot{Q}_{in}} = \frac{\dot{V}\rho c_p(T_2 - T_1)}{IA_{Col}} \tag{3}$$

As the Reynolds number for the 50:50 EG-Water solution is less than 2000, laminar flow is chosen for the CFD model. Thus, the equations for the conservation of continuity, momentum and energy are shown below.

https://doi.org/10.24191/jmeche.v23i3.9739

©Kashif Waseem et al., 2026

Continuity Equation:

$$\rho_{nf}\left(\frac{\partial u_x}{\partial x}+\frac{\partial u_y}{\partial y}+\frac{\partial u_z}{\partial z}\right)=0 \tag{4}$$

Momentum Equations:

X-Component:

$$u_x\frac{\partial u_x}{\partial x}+u_y\frac{\partial u_x}{\partial y}+u_z\frac{\partial u_x}{\partial z}=\frac{-1}{\rho_{nf}}\frac{\partial P}{\partial x}+\frac{\mu_{nf}}{\rho_{nf}}\left(\frac{\partial^2 u_x}{\partial x^2}+\frac{\partial^2 u_x}{\partial y^2}+\frac{\partial^2 u_x}{\partial z^2}\right) \tag{5}$$

Y-Component:

$$u_x\frac{\partial u_y}{\partial x}+u_y\frac{\partial u_y}{\partial y}+u_z\frac{\partial u_y}{\partial z}=g_y\beta_{nf}(T-T_\infty)+\frac{\mu_{nf}}{\rho_{nf}}\left(\frac{\partial^2 u_y}{\partial x^2}+\frac{\partial^2 u_y}{\partial y^2}+\frac{\partial^2 u_y}{\partial z^2}\right) \tag{6}$$

Z-Component:

$$u_x\frac{\partial u_z}{\partial x}+u_y\frac{\partial u_z}{\partial y}+u_z\frac{\partial u_z}{\partial z}=\frac{-1}{\rho_{nf}}\frac{\partial P}{\partial z}+\frac{\mu_{nf}}{\rho_{nf}}\left(\frac{\partial^2 u_z}{\partial x^2}+\frac{\partial^2 u_z}{\partial y^2}+\frac{\partial^2 u_z}{\partial z^2}\right) \tag{7}$$

Energy Equation:

$$\rho_{nf}c_{nf}\left(u_x\frac{\partial T}{\partial x}+u_y\frac{\partial T}{\partial y}+u_z\frac{\partial T}{\partial z}\right)=k_{nf}\left(\frac{\partial^2 T}{\partial x^2}+\frac{\partial^2 T}{\partial y^2}+\frac{\partial^2 T}{\partial z^2}\right) \tag{8}$$

The change in density is expressed using the Boussinesq Approximation:

$$\rho_{nf}=\rho_{nf0}\left[1-\beta_{nf}(T-T_0)\right] \tag{9}$$

Nanofluid Density:

$$\rho_{nf}=(1-\varphi)\rho_f+\varphi\rho_s \tag{10}$$

Nanofluid Heat Capacity:

$$c_{p(nf)}=\frac{(1-\varphi)\rho_f c_{p(f)}+\varphi\rho_s c_{p(s)}}{\rho_{nf}} \tag{11}$$

https://doi.org/10.24191/jmeche.v23i3.9739

©Kashif Waseem et al., 2026

Nanofluid Viscosity (Brinkman, 1952):

$$\mu_{nf} = \frac{\mu_f}{(1-\varphi)^{2.5}} \tag{12}$$

Nanofluid Thermal Conductivity (Maxwell, 1873):

$$\frac{k_{nf}}{k_f} = \frac{k_s + 2k_f - 2\varphi(k_f - k_s)}{k_s + 2k_f + \varphi(k_f - k_s)} \tag{13}$$

Nanofluid Thermal Expansion Coefficient (Khanafer et al., 2003):

$$\frac{\beta_{nf}}{\beta_f} = \frac{1}{1 + \frac{(1-\varphi)\rho_f}{\varphi\rho_s}} \frac{\beta_s}{\beta_f} + \frac{1}{1 + \frac{\varphi\rho_s}{(1-\varphi)\rho_f}} \tag{14}$$

The thermophysical properties of water and CuO nanoparticles are summarized in Table 3. Using Equations 10 to 14, these properties were calculated for CuO/50:50 EG–water nanofluids at volume concentrations ranging from 1% to 5% and are summarized in Table 4.

Table 3. Thermophysical properties of water and CuO nanoparticles

	ρ (kg/m^3)	c_p (J/kgK)	k (W/mK)	μ (kg/ms)	β (/K)
50% EG-Water	1073	3450	0.3736	0.0028	0.00063
CuO	6500	533	76.5	-	0.000018

Table 4. Thermophysical properties of CuO/50:50 EG-water nanofluids at different volume concentrations

φ (%)	ρ (kg/m^3)	c_p (J/kgK)	k (W/mK)	μ (kg/ms)	β (/K)
1	1127.27	3281.80	0.3848	0.002871	0.000595
2	1181.54	3129.05	0.3961	0.002945	0.000563
3	1235.81	2989.72	0.4077	0.003022	0.000533
4	1290.08	2862.11	0.4196	0.003101	0.000507
5	1344.35	2744.81	0.4317	0.003183	0.000482

Computational domain

The computational domain is displayed in Fig. 5 and boundary conditions are applied to perform the simulation. The solid surfaces of the manifold pipe are designated as walls including the inner surfaces connected to the collector tubes. A uniform heat flux corresponding to the irradiance is applied to the inner surfaces of the collector tubes. For each simulation the fluid volumetric flow rate, inlet temperature, pressure and the irradiance were specified according to the collected experimental data. Simulations were performed for the same three test days as the experiment, enabling a direct comparison between the CFD model and the measured collector performance.

https://doi.org/10.24191/jmeche.v23i3.9739

©Kashif Waseem et al., 2026

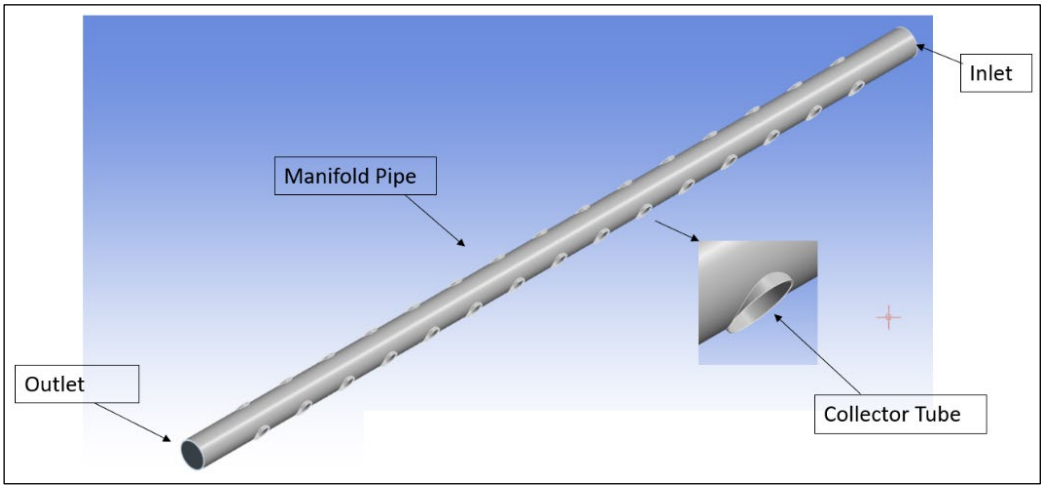


Fig. 5. Computational domain of the manifold pipe.

Mesh and mesh independence

A mesh independence test was conducted to optimize the computational efficiency for calculating the thermal performance of the ETSC. A tetrahedral mesh structure was employed, as illustrated in Fig. 6. The number of elements was varied from 0.2 million to 2.3 million across 5 tests as displayed in Fig. 7. It was observed that for element counts higher than 1.2 million, the outlet temperature of the collector exhibited behaviour independent of the mesh. Thus, 1.2 million elements were used for all subsequent simulations. Each simulation was performed with 500 iterations until convergence was achieved.

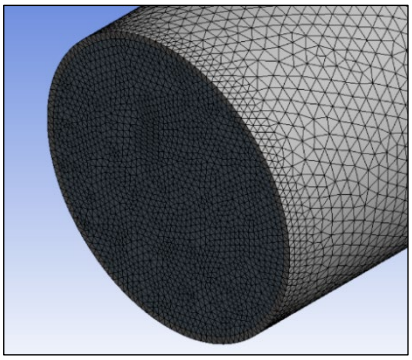


Fig. 6. Image of the mesh structure.

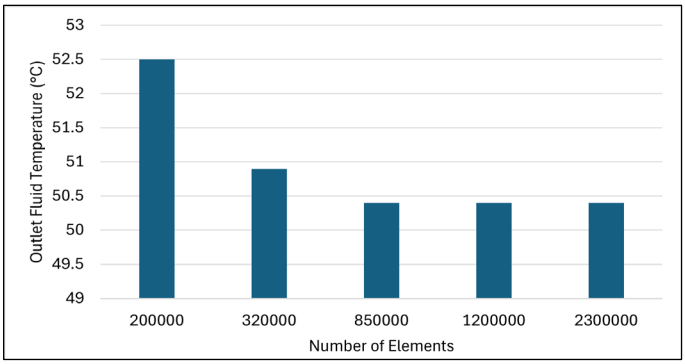


Fig. 7. Mesh independence test.

Simulation procedure

In the simulations, a finite volume approach was used to scrutinize the fluid flow in the ETSC. The SIMPLE approach was used to obtain velocity and temperature distributions, and the discretization of equations was performed using second order upwind. The Green Gauss Node method was selected for the gradient setting. The fluid was modelled as single-phase, incompressible, laminar flow while the Boussinesq Approximation was used to model the fluid density.

https://doi.org/10.24191/jmeche.v23i3.9739

©Kashif Waseem et al., 2026

Parametric optimization procedure

To achieve the third objective, the optimal operating conditions of the ETSC were determined through a structured parametric optimization framework based on DOE and Response Surface Methodology (RSM). The validated CFD model was simulated over a range of operating conditions defined by four input parameters, and the resulting output parameters were recorded. The selected input parameters were Reynolds number, *Re*, nanoparticle volume concentration, φ, irradiance, I, and collector inlet temperature, T_1. The output parameters are Nusselt number, *Nu*, and skin friction coefficient, Cf which are selected to characterize thermal performance and frictional losses, respectively.

A Central Composite Design (CCD) was implemented using Minitab to systematically generate the experimental design matrix. This resulted in a total of 31 simulation runs, including factorial points, axial points, and replicated center points. The inclusion of 6 repeated runs at the center of the design space, as shown in Table 7, serves to evaluate experimental repeatability and estimate pure error, thereby improving the statistical reliability of the model. For each input parameter, the minimum and maximum values were determined as shown in Table 5. For each of the 31 design points, the CFD model was simulated to obtain the corresponding values of *Nu* and *Cf*. Subsequently, second-order polynomial regression models were developed using RSM to capture both the individual and interaction effects of the input variables on the output responses. The adequacy and significance of the models were assessed using analysis of variance (ANOVA), including p-values at a 95% confidence level and the coefficient of determination (R^2). Sensitivity analysis was performed to identify the most influential input parameters affecting *Nu* and *Cf*. Finally, a composite desirability approach was employed to determine the optimal combination of input parameters that simultaneously maximized thermal performance while minimizing frictional losses.

Table 5. Minimum, mean and maximum values of the input parameters

	Min	Mean	Max
Re	85	467.5	850
φ (%)	0	2.5	5
I (W/m^2)	300	650	1000
T_1 (K)	283	298	313

Results and Discussion

Model validation

Figs. 8 and 9 present the comparison between the experimental and CFD-simulated outlet fluid temperatures and thermal efficiencies for the three test days. Additionally, the percentage errors for T_2 and η were calculated to assess the accuracy of the CFD model as summarized in Table 6.

Fig. 8 compares the outlet fluid temperatures of the experiment and the simulation model. It is evident that $T_{2,sim}$ is very close to $T_{2,exp}$ across all 3 days, with the maximum percentage error being 2.33% for Day 1 and the minimum percentage error being 1.05% for Day 2. This consistently low error range strongly validates the simulation model, confirming its accurate $T_{2,sim}$ values. Likewise, Fig. 9 compares the collector's thermal efficiency for the experiment and CFD model. It is clear that η_{sim} is close to η_{exp} for each of the three days with the lowest and highest percentage error being 2.94% and 9.19% for Days 2 and 3 respectively. These low error values in η further validate the CFD model demonstrating its accurate thermal efficiency values.

https://doi.org/10.24191/jmeche.v23i3.9739

©Kashif Waseem et al., 2026

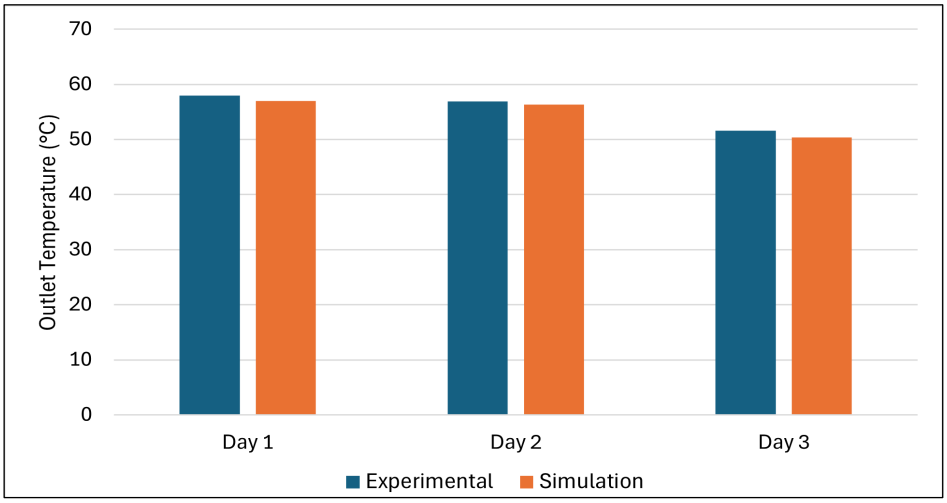


Fig. 8. Comparison of experimental and simulated outlet temperatures.

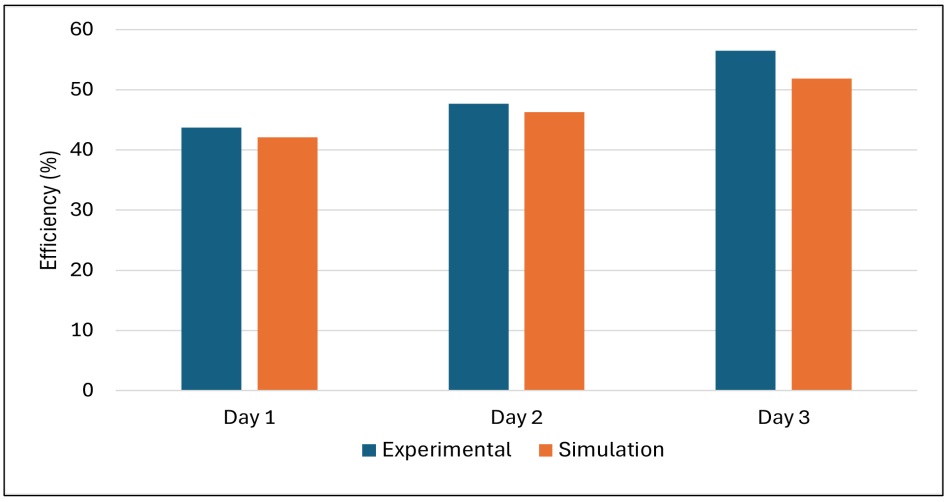


Fig. 9. Comparison of experimental and simulated collector efficiency.

Table 6. Comparison of experimental and CFD simulation results

Day	$T_{2,exp}$ $(°C)$	$T_{2,sim}$ $(°C)$	$\%Error$ in T_2	ΔT_{exp} $(°C)$	ΔT_{sim} $(°C)$	η_{exp} (%)	η_{sim} (%)	% $Error$ in η
Day 1	58	57	1.72%	28	27	43.7	42.1	3.66%
Day 2	56.9	56.3	1.05%	20.6	20	47.7	46.3	2.94%
Day 3	51.6	50.4	2.33%	14.6	13.4	56.5	51.9	9.19%

https://doi.org/10.24191/jmeche.v23i3.9739

©Kashif Waseem et al., 2026

Simulation with CuO nanofluids

The CFD model on Day 2 yielded the lowest percentage error of 1.05% and was therefore selected for simulation with CuO nanofluids. The simulations were performed across a range of volumetric flow rates and nanoparticle volume concentrations to evaluate their influence on the collector's thermal performance.

Effect on Nusselt number and skin friction coefficient

Fig. 10 displays the relationship between the Nusselt number and Reynolds number for 50:50 EG-water and 5% CuO/50:50 EG-water nanofluid. For both fluids, Nusselt number increases at higher Reynolds number, consistent with the stronger influence of forced convection at higher flow rates. At any given *Re,* however, the nanofluid consistently exhibits higher values of *Nu* compared to the base fluid confirming its superior heat transfer properties. This enhancement is primarily attributed to the higher thermal conductivity of the CuO-based nanofluid, as well as to collisions between the nanoparticles and the manifold pipe wall, which results in additional heat transfer (Sarkar et al., 2024; Tian et al., 2023). Notably, the enhancement in *Nu* becomes more pronounced at higher *Re.* For example, at *Re* = 85, the enhancement in *Nu* achieved using 5% CuO/50:50 EG–Water is 5% compared to the base fluid, while at *Re* = 850 the improvement is 34%. These findings indicate that utilization of nanofluids is particularly advantageous at high flow rates where convective heat transfer is enhanced and ETSC thermal performance can be maximized.

Fig. 11 shows the influence of nanoparticle volume concentration (φ=1%-5%) on *Nu* as a function of *Re*. It is evident that higher nanoparticle concentrations result in increased *Nu*, thereby improving the thermal performance of the ETSC. The maximum enhancement occurs at φ=5% where the superior thermal conductivity of the nanofluid yields the greatest improvement in heat transfer. At *Re*=85, the Nusselt number for φ=5% is 4.4% higher than for φ=1%, while at *Re*=850 the corresponding enhancement is 25.9%. This further underlines that nanoparticle concentration has a stronger effect under high Reynolds number, highlighting the importance of optimizing both flow regime and concentration to maximize thermal performance.

Fig. 12 illustrates the variation of skin friction coefficient against Reynolds number for the base fluid and 5% CuO/50:50 EG-Water. For both fluids, It is observed that *Cf* decreases with increasing *Re*, confirming the reduced relative shear stress at higher flow rates. Nevertheless, the nanofluid exhibits consistently higher *Cf* values due to its higher viscosity, which leads to increased frictional losses. Additionally, collisions between the nanoparticles and manifold pipe wall result in increased shear stress, thereby further contributing to higher *Cf* values for the nanofluid. At *Re*=850, the skin friction coefficient of the 5% nanofluid is 21.4% greater than that of the base fluid, reflecting the increase in thermal losses associated with nanoparticle addition.

Fig. 13 presents *Cf* as a function of *Re* for varying nanoparticle volume concentrations (φ=1%-5%). For any given *Re* value, *Cf* increases with increasing volume concentration, with the 5% nanofluid exhibiting the highest values. At *Re*=850, the *Cf* of the 5% nanofluid is 15.8% higher than that of the 1% nanofluid, demonstrating that viscosity rise with concentration directly impacts frictional losses. These findings highlight the trade-off between enhanced heat transfer and increased frictional losses, underscoring the importance of optimizing nanoparticle concentration to balance thermal benefits with hydraulic penalties.

These results are consistent with those reported by Hasan et al. (2022), who observed similar trends for the Nusselt number and skin friction coefficient with respect to the Reynolds number. In their study, the maximum *Nu* enhancement was 42% at *Re*=30000 using SiO_2 nanofluids (φ=4%) compared to water. The higher degree of *Nu* enhancement reported in their work can be attributed to the significantly larger Reynolds numbers investigated relative to those considered in the present study. Similarly, their findings for *Cf* confirmed that the use of nanofluids consistently increased frictional losses due to elevated viscosity,

https://doi.org/10.24191/jmeche.v23i3.9739

©Kashif Waseem et al., 2026

which is in agreement with the present results. The consistency with existing literature supports the reliability of the CFD model and the accuracy of the results.

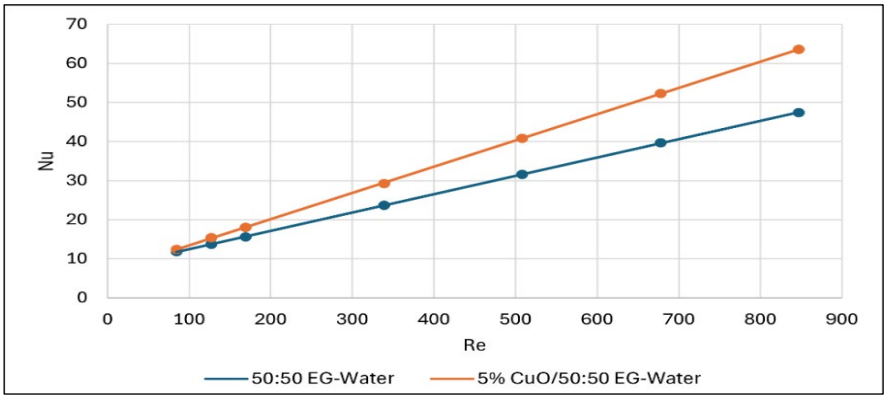


Fig. 10. Nusselt Number vs Reynolds Number using 50:50 EG-Water and 5% CuO/50:50 EG-Water.

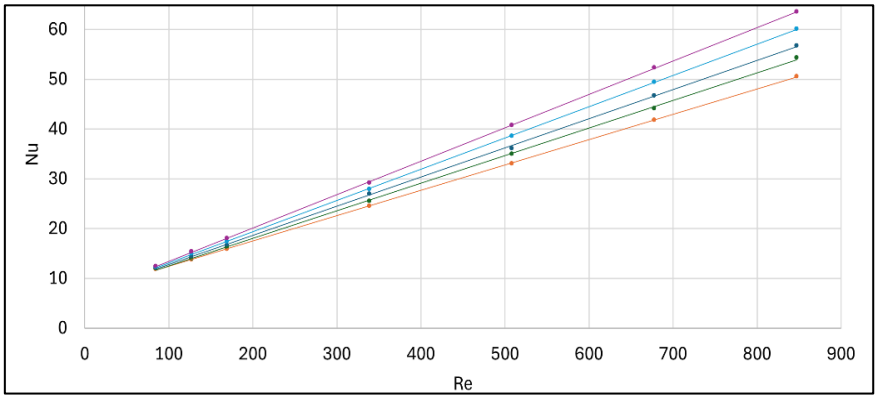


Fig. 11. Nusselt Number vs Reynolds Number for different volume concentrations of CuO/50:50 EG-Water.

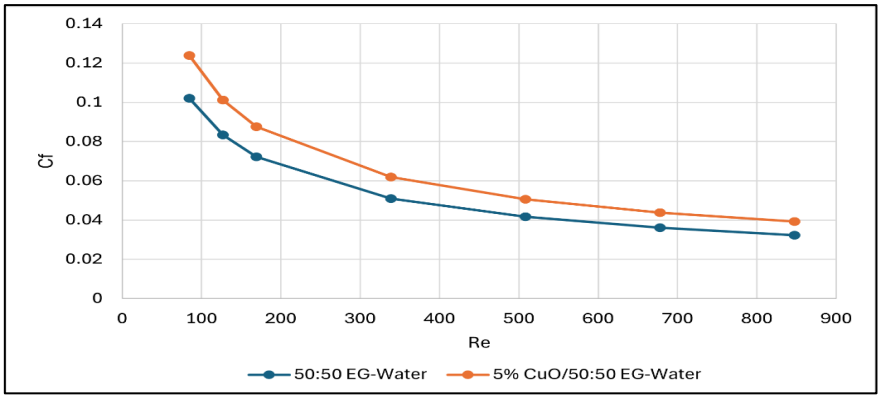


Fig. 12. Skin friction coefficient vs Reynolds Number using 50:50 EG-Water and 5% CuO/50:50 EG-Water.

https://doi.org/10.24191/jmeche.v23i3.9739

©Kashif Waseem et al., 2026

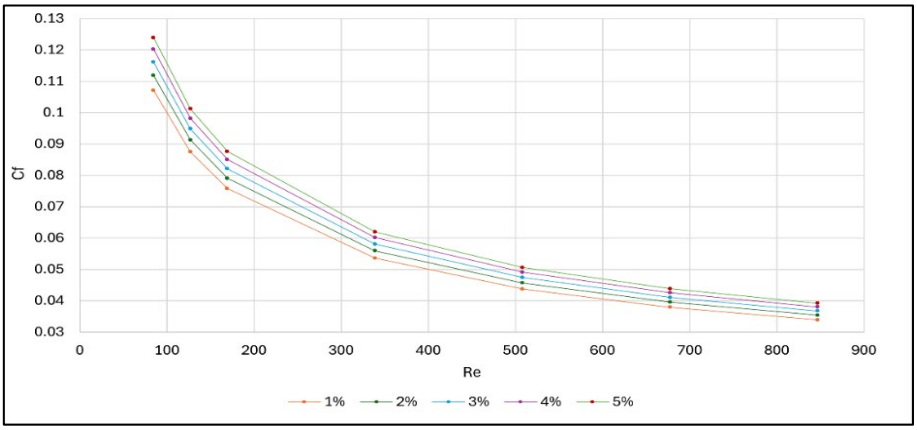


Fig. 13. Variation of skin friction coefficient with Reynolds Number for different volume concentrations of CuO/50:50 EG-Water.

Effect on ETSC thermal efficiency

Fig. 14 illustrates the variation of collector efficiency with reduced temperature at different nanoparticle volume concentrations. As the reduced temperature increases, η decreases almost linearly. This trend arises from greater heat losses to the surroundings at higher mean fluid temperatures, which reduce the overall collector efficiency. At $\frac{T_m - T_a}{I} = 0$, the collector thermal efficiency with 5% CuO/50:50 EG-Water is 58.8% representing a 13.1% enhancement compared to using the base fluid (52%). It is also evident that higher nanoparticle concentrations yield greater η values, confirming that the thermal performance of the ETSC improves as φ increases.

This is further supported by Fig. 15 which presents thermal efficiency of the ETSC as a function of solar irradiance for different φ values. At low irradiance values, η increases sharply for all volume concentrations. Beyond I = 200 W/m^2, however, the rate of growth of η diminishes and eventually approaches a near-constant slope as the collector approaches its thermal performance limit. As a result, although the useful heat gain continues to rise with irradiance, it does so at a diminishing rate compared to the increase in the heat input, causing the efficiency curve to flatten. Across all irradiance levels, the 5% nanofluid achieves the highest efficiency, showing enhancements of 10.8% at I = 100 W/m^2 and 13.5% at I = 1000 W/m^2 compared to the base fluid. These findings reinforce that both higher nanoparticle concentrations and increased irradiance significantly improve ETSC thermal performance.

https://doi.org/10.24191/jmeche.v23i3.9739

©Kashif Waseem et al., 2026

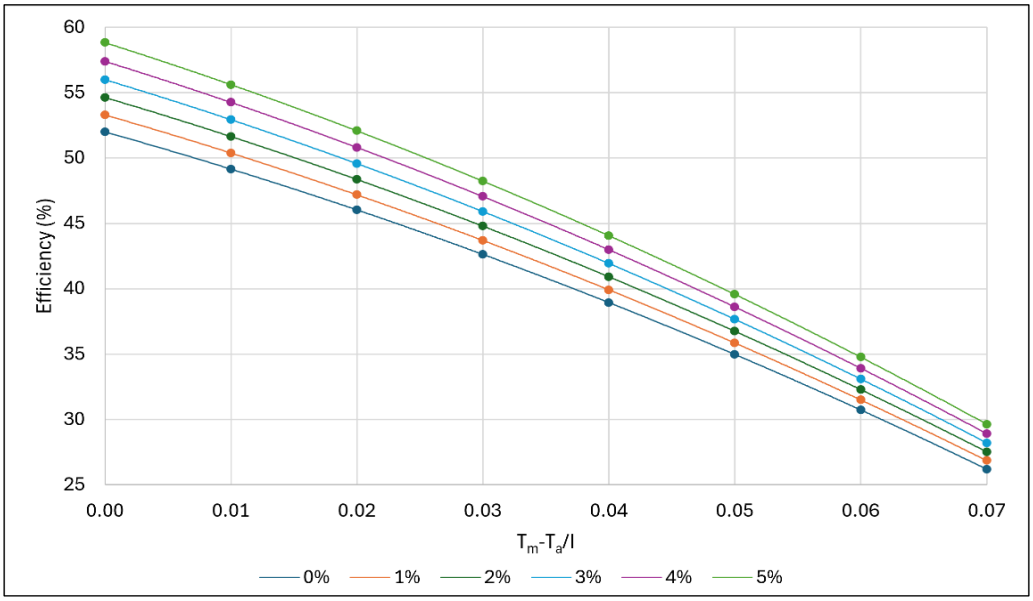


Fig. 14. Collector thermal efficiency vs reduced temperature for different volume concentrations of CuO/50:50 EG-Water.

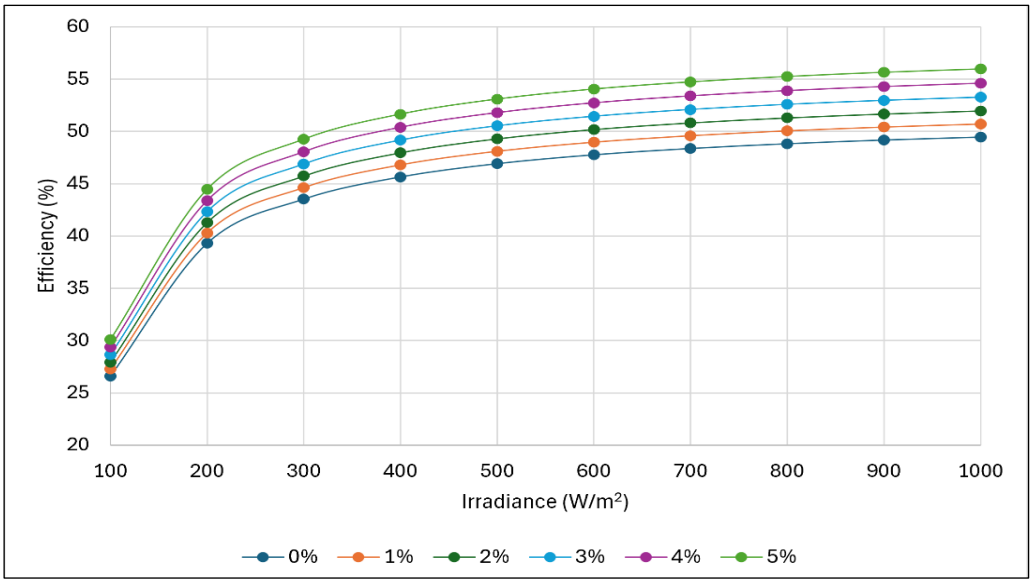


Fig. 15. Collector thermal efficiency vs irradiance using various volume concentrations of CuO/50:50 EG-Water.

These results are in agreement with those reported in the literature. As shown in Fig. 1, Mercan & Yurddas (2019) reported a maximum enhancement in thermal efficiency of 6.8% using 5% CuO/Water as the ETSC working fluid while Kim et al. (2016) achieved a 6.1% increase with 3% CuO/20:80 PG–Water. Peng et al. (2020) reported a higher enhancement of 13.8% using 4% CuO/Water. The higher thermal efficiency enhancement of 13.5% obtained in the present study exceeds that of Mercan & Yurddas (2019)

https://doi.org/10.24191/jmeche.v23i3.9739

©Kashif Waseem et al., 2026

due to the higher applied irradiance (1000 W/m^2 compared to 800 W/m^2). Similarly, it also surpasses that of Kim et al. (2016) likely due to their use of a lower nanoparticle concentration (3% vs. 5%). Conversely, the slightly greater enhancement achieved by Peng et al. (2020) despite a lower nanoparticle concentration (4%) may be explained by their use of a larger 94 mm diameter collector tube compared to the 42 mm manifold pipe in this study. A larger diameter reduces flow resistance and associated pressure drop, which can enhance overall thermal performance. In contrast, smaller diameters typically exhibit a higher area-to-volume ratio, which promotes increased convective heat transfer due to enhanced surface interaction. However, this improvement is often offset by higher frictional losses and pressure drops, which can limit the effective heat transfer enhancement compared to larger diameters. Therefore, the larger diameter tube used by Peng et al. (2020) may have contributed to improved heat transfer performance of the ETSC compared to the present study.

Parametric optimization

Regression analysis

In total, 31 simulations were performed and the corresponding values of Nusselt number and skin friction coefficient were recorded, with the results presented in Table 7. The results were statistically analysed to generate an equation for calculated *Nu* and *Cf* values.

Equation for Nusselt Number:

$$Nu = 17.3 + 0.0287Re - 1.367\varphi - 0.01I - 0.0209T_1 + 0.000003Re^2 + 0.002252Re\varphi + 0.000021ReI - 0.000002\ ReT_1 + 0.001996\varphi I + 0.000016IT_1 \quad (15)$$

For Skin Friction Coefficient:

$$Cf = 0.2108 - 0.000307Re + 0.003704\varphi - 0.000057I - 0.000359T_1 + 0.00000017Re^2 - 0.000004Re\varphi + 0.0000001\ ReT_1 + 0.0000009\varphi I\ + 0.00000024IT_1 \quad (16)$$

Table 7. Results of parametric optimization

Simulation	*Re*	φ (%)	*I* (W/m^2)	T_1 (K)	*Nu*	*Cf*
1	85	0	300	283	10.99	0.09499
2	85	0	300	313	10.39	0.08479
3	85	0	1000	283	11.88	0.10321
4	85	0	1000	313	11.81	0.10203
5	85	2.5	650	298	11.71	0.10945
6	85	5	300	283	11.27	0.11490
7	85	5	300	313	10.94	0.10260
8	85	5	1000	283	12.49	0.12453
9	85	5	1000	313	12.43	0.12391
10	467.5	0	650	298	27.83	0.03929
11	467.5	2.5	650	298	30.29	0.04510
12	467.5	2.5	650	298	30.29	0.04510
13	467.5	2.5	650	298	30.29	0.04510
14	467.5	2.5	650	298	30.29	0.04510
15	467.5	2.5	650	298	30.29	0.04510

https://doi.org/10.24191/jmeche.v23i3.9739

©Kashif Waseem et al., 2026

16	467.5	2.5	650	298	30.29	0.04510
17	467.5	2.5	650	298	30.29	0.04510
18	467.5	2.5	300	298	27.24	0.04132
19	467.5	2.5	650	328	29.98	0.04465
20	467.5	2.5	650	268	30.61	0.04562
21	467.5	2.5	1350	298	34.84	0.05271
22	467.5	5	650	298	32.89	0.05112
23	850	0	300	283	42.18	0.02854
24	850	0	300	313	41.74	0.02840
25	850	0	1000	283	47.75	0.03261
26	850	0	1000	313	47.43	0.03227
27	850	2.5	650	298	52.89	0.03386
28	850	5	300	283	44.43	0.03156
29	850	5	300	313	43.97	0.03042
30	850	5	1000	283	63.92	0.03934
31	850	5	1000	313	63.59	0.03918

Using Equations 15 and 16, regression plots are produced for *Nu* and *Cf* as shown in Figs. 16 and 17 respectively. Fig. 16 presents the regression plot for the Nusselt number, where the data points closely align with the line of best fit, yielding a high R^2 value of 0.9917, underlining the accuracy and validity of the simulated *Nu* values. This is further reflected in Fig. 17 which displays the regression plot for the skin friction coefficient. The slope of the plot is approximately unity, and the R^2 value is 0.9816, further confirming the accuracy of the input parameters and boundary conditions employed in the CFD model. The close alignment of the calculated and simulated values of *Nu* and *Cf* validates both the accuracy of the CFD model as well as the reliability of Equations 15 and 16 for predicting *Nu* and *Cf* across varying input conditions.

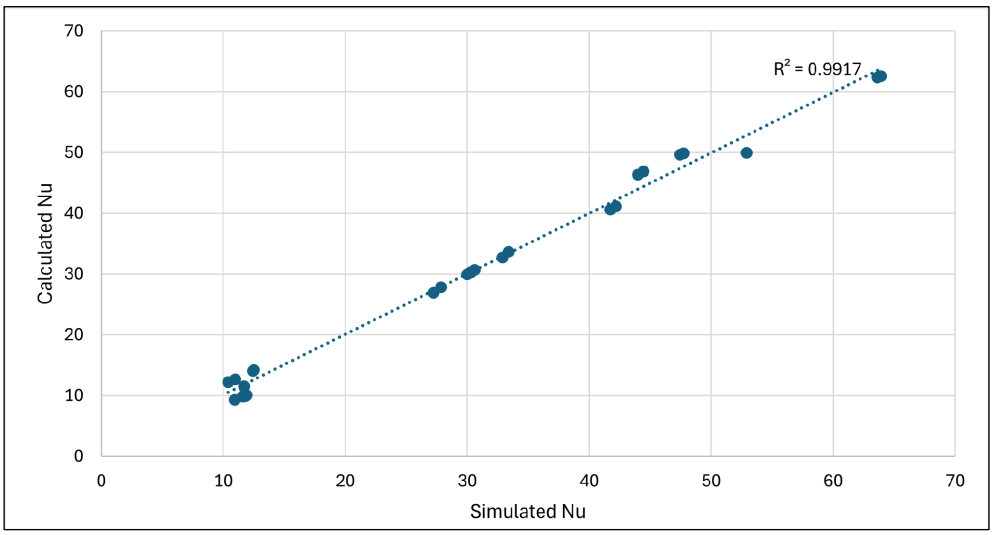


Fig. 16. Regression plot for calculated vs simulated Nusselt Number values.

https://doi.org/10.24191/jmeche.v23i3.9739

©Kashif Waseem et al., 2026

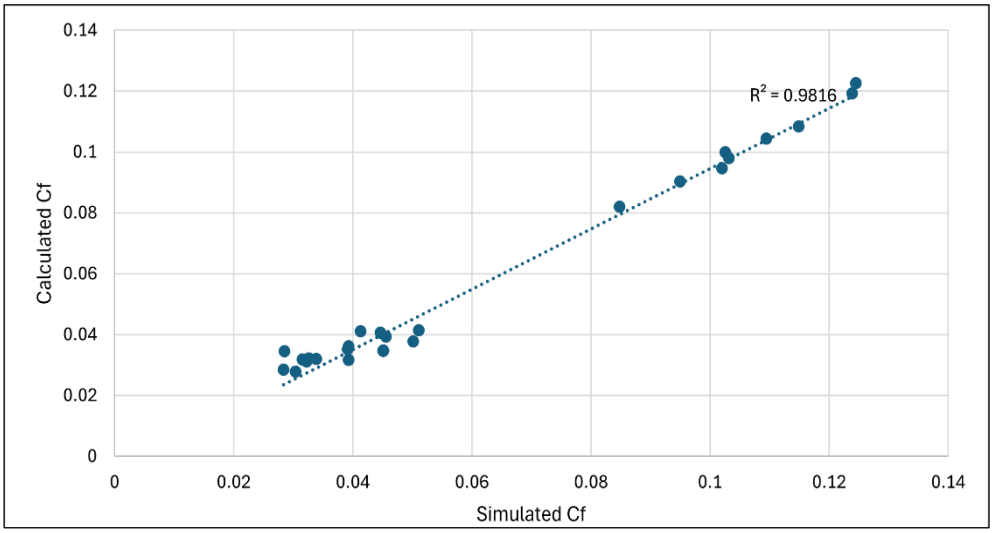


Fig. 17. Regression plot for calculated vs simulated skin friction coefficient values.

Sensitivity analysis

Sensitivity analysis is performed to quantify the change in output parameters with respect to the input parameters and their relative significance. This analysis identifies the optimal combination of input parameters for enhancing ETSC thermal performance by maximizing *Nu* and minimizing *Cf*. Equations 15 and 16 can subsequently be partially differentiated with respect to the input parameters (Re, φ, I, T_1), to determine the sensitivities of *Nu* and *Cf*.

For Nusselt Number:

$$\frac{\partial Nu}{\partial Re} = 0.0287 + 0.000006Re + 0.002252\varphi + 0.000021I - 0.000002T_1 \quad (17)$$

$$\frac{\partial Nu}{\partial \varphi} = -1.367 + 0.002252Re + 0.001996I \quad (18)$$

$$\frac{\partial Nu}{\partial I} = -0.01 + 0.000021Re + 0.001996\varphi + 0.000016T_1 \quad (19)$$

$$\frac{\partial Nu}{\partial T_1} = -0.0209 - 0.000002Re + 0.000016I \quad (20)$$

For Skin Friction Coefficient:

$$\frac{\partial Cf}{\partial Re} = -0.000307 + 0.00000034Re - 0.000004\varphi + 0.0000001T_1 \quad (21)$$

$$\frac{\partial Cf}{\partial \varphi} = 0.003704 - 0.000004Re + 0.0000009I \quad (22)$$

$$\frac{\partial Cf}{\partial I} = -0.000057 + 0.0000009\varphi + 0.00000024T_1 \quad (23)$$

https://doi.org/10.24191/jmeche.v23i3.9739

©Kashif Waseem et al., 2026

$$\frac{\partial Cf}{\partial T_1} = -0.000359 + 0.0000001Re + 0.00000024I \quad (24)$$

Equations 17 to 24 present the partial derivatives of *Nu* and *Cf* with respect to the input parameters. By substituting the input values from Table 5 into these equations, the sensitivities of the output parameters are obtained, where a positive value indicates that the output increases with an increase in the corresponding input, and a negative value indicates the opposite. The calculated sensitivities are shown in Tables 8 and 9 for various combinations of the input parameters.

Table 8. Nusselt Number sensitivities of input parameters

Re	φ	I	T_1	$\frac{\partial Nu}{\partial Re}$	$\frac{\partial Nu}{\partial \varphi}$	$\frac{\partial Nu}{\partial I}$	$\frac{\partial Nu}{\partial T_1}$
850	5	1000	313	0.065434	2.5432	0.022838	-0.0066
850	5	1000	298	0.065464	2.5432	0.022598	-0.0066
850	5	1000	283	0.065494	2.5432	0.022358	-0.0066
467.5	5	1000	283	0.063199	1.6818	0.014326	-0.0058
467.5	2.5	1000	283	0.057569	1.6818	0.014326	-0.0058

Table 9. Skin friction coefficient sensitivities of input parameters

Re	φ	I	T_1	$\frac{\partial Cf}{\partial Re}$	$\frac{\partial Cf}{\partial \varphi}$	$\frac{\partial Cf}{\partial I}$	$\frac{\partial Cf}{\partial T_1}$
850	5	1000	313	-0.0000067	0.001204	0.00002902	-0.000034
850	5	1000	298	-0.0000082	0.001204	0.00002262	-0.000034
850	5	1000	283	-0.0000097	0.001204	0.00001542	-0.000034
467.5	5	1000	283	-0.0001398	0.002734	0.00001542	-0.000025
467.5	2.5	1000	283	-0.0001298	0.002734	0.00001317	-0.000025

Results indicate that φ and I have positive sensitivities, which means that increasing these parameters increases *Nu* and *Cf*. In contrast, T_1 exhibits negative sensitivity for both outputs, where higher collector inlet temperatures reduce *Nu* and *Cf*. Lastly, the Reynolds number exhibits a positive sensitivity on *Nu* but a negative sensitivity on *Cf* which means that increasing *Re* enhances heat transfer while reducing frictional losses. These results corroborate those obtained from the CFD model, reinforcing the robustness of the sensitivity analysis. In terms of magnitude, *Nu* is most sensitive to φ and least sensitive to T_1. Similarly, *Cf* is also most sensitive to φ but is least sensitive to *Re*. Thus, φ is the most influential input parameter affecting the thermal performance of the ETSC.

Optimal input parameters

Table 10 presents the optimal input parameters for maximizing the thermal performance of the ETSC. The optimal conditions are Re = 850, φ = 5%, I = 1000 W/m^2 and T_1 = 268 K. It is noted that the optimal inlet temperature pf T_1 = 268 K lies below the minimum experimentally tested value of T_1 = 283 K. This is because the RSM provides a continuous approximation of the response surface and enables prediction of optimal conditions within the design space, but beyond the experimentally tested range. As a result, the optimization process may identify optima slightly beyond the experimentally tested range from Table 5.

This combination of parameters yields superior thermal performance, achieving maximum heat transfer and minimal frictional losses in the ETSC. Under these conditions, the Nusselt number is 62.6 underscoring

https://doi.org/10.24191/jmeche.v23i3.9739

©Kashif Waseem et al., 2026

the enhanced thermophysical properties of 5% CuO/50:50 EG-water, while the skin friction coefficient of 0.0359 is low and highlights minimal energy losses due to friction in the ETSC.

Table 10. Optimal input parameters and corresponding output values

Re	φ (%)	I (W/m^2)	T_1 (K)	*Cf* fit	*Nu* fit	Composite Desirability
850	5	1000	268	0.0359156	62.5767	0.947991

Conclusion

The present study successfully evaluated the thermal performance of the ETSC using CuO/50:50 EG-water nanofluids through experimental, computational and numerical methods. The experimental results provided essential data for validating the CFD model. The simulated fluid outlet temperatures aligned closely with experimental values with minimum and maximum percentage errors of 1.05% and 2.33% respectively. These low errors affirmed the accuracy and reliability of the CFD model.

Utilizing CuO/50:50 EG-water nanofluids as the collector working fluid at various volume concentrations (φ=1%-5%) enhanced the heat transfer of the ETSC. At φ=5%, the Nusselt number increased by 34% compared to the base fluid, indicating enhanced heat transfer. At the same concentration, the skin friction coefficient increased by 21.4% representing higher thermal losses when using nanofluids. Furthermore, increasing φ improved the thermal performance of the collector due to the higher thermal conductivity of the nanofluid. Thus, the thermal efficiency of the ETSC improved with increasing CuO volume concentration. Using 5% CuO/50:50 EG-Water, the maximum thermal efficiency enhancement was 13.5% compared to 50:50 EG-Water, demonstrating the strong potential of CuO nanofluids to enhance ETSC thermal performance.

Parametric optimization and sensitivity analysis revealed that increasing nanoparticle volume concentration and irradiance positively influenced both Nusselt number and skin friction coefficient, while increasing collector inlet temperature had a negative effect. Reynolds number exhibited a positive impact on *Nu* but a negative influence on *Cf*. The optimal combination of input parameters was determined to occur at Re = 850, φ = 5%, I = 1000 W/m^2, and T_1 = 268 K. Under these conditions, *Nu* in the ETSC was 62.6 and *Cf* was 0.0359, highlighting high thermal performance and minimal energy losses. The study concludes that incorporating CuO nanofluids into ETSCs significantly improves heat transfer and collector thermal efficiency, demonstrating their strong potential for enhancing ETSC thermal performance.

Acknowledgements/ Funding

The authors would like to acknowledge the support of Heriot Watt University Dubai, Dubai, UAE, for providing the facilities for this research.

Conflict of Interest Statement

All authors declare that they have no conflicts of interest.

https://doi.org/10.24191/jmeche.v23i3.9739

©Kashif Waseem et al., 2026

Authors' Contributions

The authors confirm their contribution to the paper as follows: study conception and design: Kashif Waseem, Ahmed N. Oumer; data collection: Kashif Waseem; analysis and interpretation of results: Kashif Waseem, Ahmed N. Oumer, Rehan Ahmed; draft manuscript preparation: Kashif Waseem. All authors reviewed the results and approved the final version of the manuscript.

Data Availability/Supplementary Materials

The datasets used and/or analyzed during the current study are available from the corresponding author on reasonable request.

Ethics Statement

The authors declare that this research did not involve human or animal subjects. All experimental procedures were performed following the institutional Safety, Health, and Environmental (HSE) protocols of Heriot Watt University Dubai.

Reference

Aggarwal, S., Kumar, R., Lee, D., Kumar, S., & Singh, T. (2023). A comprehensive review of techniques for increasing the efficiency of evacuated tube solar collectors. Heliyon, 9(4), e15185. https://doi.org/10.1016/j.heliyon.2023.e15185

Ayompe, L. M., & Duffy, A. (2013). Thermal performance analysis of a solar water heating system with heat pipe evacuated tube collector using data from a field trial. Solar Energy, 90, 17-28. https://doi.org/10.1016/j.solener.2013.01.001

Aytaç, İ., Khanlari, A., Tuncer, A. D., Variyenli, H. İ., & Ünvar, S. (2024). Performance improvement of a heat pipe evacuated solar water collector using quartz/water nanofluid: a numerical and experimental study. Renewable Energy, 236, 121423. https://doi.org/10.1016/j.renene.2024.121423

Brinkman, H. C. (1952). The viscosity of concentrated suspensions and solutions. The Journal of Chemical Physics, 20(4), 571. https://doi.org/10.1063/1.1700493

Cheng, X. M., Zhu, C., Zhang, H., & Yang, X. J. (2013). Research and application of heat transfer fluids in solar thermal power. Advanced Materials Research, 815, 415–422. https://doi.org/10.4028/www.scientific.net/AMR.815.415

Hasan, H. A., Sherza, J. S., Abed, A. M., Sultan, H. S., & Sopian, K. (2022). Improve the performance of solar thermal collectors by varying the concentration and nanoparticles diameter of silicon dioxide. Open Engineering, 12(1), 743-751. https://doi.org/10.1515/eng-2022-0339

Jaiswal, P., Kumar, Y., Das, L., Mishra, V., Pagar, R., Panda, D., & Biswas, K. G. (2023). Nanofluids guided energy-efficient solar water heaters: recent advancements and challenges ahead. Materials Today Communications, 37, 107059. https://doi.org/10.1016/j.mtcomm.2023.107059

Kalogirou, S. A. (2004). Solar thermal collectors and applications. Progress in Energy and Combustion

©Kashif Waseem et al., 2026

Science, 30(3), 231-295. https://doi.org/10.1016/j.pecs.2004.02.001

Kannan, N., & Vakeesan, D. (2016). Solar energy for future world: - a review. Renewable and Sustainable Energy Reviews, 62, 1092-1105. https://doi.org/10.1016/j.rser.2016.05.022

Kaya, H., & Arslan, K. (2019). Numerical investigation of efficiency and economic analysis of an evacuated U-tube solar collector with different nanofluids. Heat and Mass Transfer, 55(3), 581-593. https://doi.org/10.1007/s00231-018-2442-z

Khanafer, K., Vafai, K., & Lightstone, M. (2003). Buoyancy-driven heat transfer enhancement in a two-dimensional enclosure utilizing nanofluids. International Journal of Heat and Mass Transfer, 46(19), 3639-3653. https://doi.org/10.1016/S0017-9310(03)00156-X

Kim, H., Ham, J., Park, C., & Cho, H. (2016). Theoretical investigation of the efficiency of a U-tube solar collector using various nanofluids. Energy, 94, 497-507. https://doi.org/10.1016/j.energy.2015.11.021

López-Núñez, O. A., Alfaro-Ayala, J. A., Ramírez-Minguela, J. J., Cano-Banda, F., Ruiz-Camacho, B., & Belman-Flores, J. M. (2022). Numerical analysis of the thermo-hydraulic performance and entropy generation rate of a water-in-glass evacuated tube solar collector using TiO2 water-based nanofluid and only water as working fluids. Renewable Energy, 197, 953-965. https://doi.org/10.1016/j.renene.2022.07.156

López-Núñez, O. A., Lara, F., González-Angeles, A., Cardenas-Robles, A., Ramírez-Minguela, J. J., & Alfaro-Ayala, J. A. (2024). Assessment of thermohydraulic performance and entropy generation in an evacuated tube solar collector employing pure water and nanofluids as working fluids. Heliyon, 10(8), e29309. https://doi.org/10.1016/j.heliyon.2024.e29309

Mangal, D., Lamba, D. K., Gupta, T., & Jhamb, K. (2010). Acknowledgement of evacuated tube solar water heater over flat plate solar water heater. International Journal of Engineering, 4(4), 279-284.

Maxwell, J. C. (1873). A treatise on electricity and magnetism (pp. 3408-3425). Clarendon Press.

Mercan, M., & Yurddaş, A. (2019). Numerical analysis of evacuated tube solar collectors using nanofluids. Solar Energy, 191, 167-179. https://doi.org/10.1016/j.solener.2019.08.074

Morrison, G. L., Budihardjo, I., & Behnia, M. (2004). Water-in-glass evacuated tube solar water heaters. Solar Energy, 76(1-3), 135-140. https://doi.org/10.1016/j.solener.2003.07.024

Nie, B., Palacios, A., Zou, B., Liu, J., Zhang, T., & Li, Y. (2020). Review on phase change materials for cold thermal energy storage applications. Renewable and Sustainable Energy Reviews, 134, 110340. https://doi.org/10.1016/j.rser.2020.110340

Olfian, H., Ajarostaghi, S. S. M., & Ebrahimnataj, M. (2020). Development on evacuated tube solar collectors: a review of the last decade results of using nanofluids. Solar Energy, 211, 265-282. https://doi.org/10.1016/j.solener.2020.09.056

Pawar, V. R., & Sobhansarbandi, S. (2020). CFD modeling of a thermal energy storage based heat pipe evacuated tube solar collector. Journal of Energy Storage, 30, 101528. https://doi.org/10.1016/j.est.2020.101528

Peng, Y., Zahedidastjerdi, A., Abdollahi, A., Amindoust, A., Bahrami, M., Karimipour, A., & Goodarzi, M. (2020). Investigation of energy performance in a U-shaped evacuated solar tube collector using oxide added nanoparticles through the emitter, absorber and transmittal environments via discrete ordinates radiation method. Journal of Thermal Analysis and Calorimetry, 139(4), 2623-2631. https://doi.org/10.1007/s10973-019-08684-w

https://doi.org/10.24191/jmeche.v23i3.9739

©Kashif Waseem et al., 2026

Raimi, D., Zhu, Y., Newell, R. C., Prest, B. C., & Bergman, A. (2023). Global energy outlook 2023: sowing the seeds of an energy transition. Resources for the Future. https://www.rff.org/publications/reports/global-energy-outlook-2023/

Sadeghi, G., Safarzadeh, H., & Ameri, M. (2019). Experimental and numerical investigations on performance of evacuated tube solar collectors with parabolic concentrator, applying synthesized Cu2O/distilled water nanofluid. Energy for Sustainable Development, 48, 88-106. https://doi.org/10.1016/j.esd.2018.10.008

Sarkar, S., Pal, P., & Ghosh, N. K. (2024). Enhancing the thermal conductivity and viscosity of ethylene glycol-based single-walled carbon nanotube (SWCNT) nanofluid: an investigation utilizing equilibrium molecular dynamics simulation. Chemical Thermodynamics and Thermal Analysis, 16, 100142. https://doi.org/10.1016/j.ctta.2024.100142

Solangi, K. H., Islam, M. R., Saidur, R., Rahim, N. A., & Fayaz, H. (2011). A review on global solar energy policy. Renewable and Sustainable Energy Reviews, 15(4), 2149-2163. https://doi.org/10.1016/j.rser.2011.01.007

Sood, T., Lee, D., Kumar, R., & Ağbulut, Ü. (2026). A detailed review of evacuated tube solar collectors for sustainable energy, current trends and future prospects. Solar Energy, 303, 114054. https://doi.org/10.1016/j.solener.2025.114054

Tabarhoseini, S. M., & Sheikholeslami, M. (2022). Modeling of evacuated tube solar collector involving longitudinal fins and nanofluids. Sustainable Energy Technologies and Assessments, 53(B), 102587. https://doi.org/10.1016/j.seta.2022.102587

Tian, W., Bao, Y., Qin, G., Liu, L., & Zheng, X. (2023). Influence mechanism of functionalization of CNTs on the thermal transport property of their nanofluids. Journal of Molecular Liquids, 392(1), 123433. https://doi.org/10.1016/j.molliq.2023.123433

Yan, S., Wang, F., Shi, Z., & Tian, R. (2017). Heat transfer property of SiO2/water nanofluid flow inside solar collector vacuum tubes. Applied Thermal Engineering, 118, 385-391. https://doi.org/10.1016/j.applthermaleng.2017.02.108

Yurddaş, A. (2020). Optimization and thermal performance of evacuated tube solar collector with various nanofluids. International Journal of Heat and Mass Transfer, 152, 119496. https://doi.org/10.1016/j.ijheatmasstransfer.2020.119496

Zubriski, S. E., & Dick, K. J. (2012). Measurement of the efficiency of evacuated tube solar collectors under various operating conditions. Journal of Green Building, 7(3), 114-130. https://doi.org/10.3992/jgb.7.3.114



© 2026 by the authors. This article is an open access article distributed under the terms and conditions of the Creative Commons Attribution (CC BY-NC-SA) license (https://creativecommons.org/licenses/by-nc-sa/4.0/)

https://doi.org/10.24191/jmeche.v23i3.9739

©Kashif Waseem et al., 2026